Wood Science and Technology (2025) 59:42
https://doi.org/10.1007/s00226-025-01645-7

ORIGINAL

Exploring wood as a sustainable solution for water filtration: nanoparticle removal, size exclusion and molecular adsorption

Antoni Sánchez-Ferrer[1] · **Jenifer Guerrero Parra**[1]

Received: 12 December 2024 / Accepted: 24 February 2025

Abstract

In regions where microbial contamination of groundwater and surface water remains a significant public health concern, leading to around 505,000 annual deaths, there is an urgent need for accessible, cost-effective, and simple household water treatment solutions. This study investigated the feasibility of wood as a filtration system, with a focus on its ability to remove nanoparticles. The research underscores the remarkable potential of wood filters, particularly in radial and tangential directions, exhibiting superior particle removal capabilities (>99%) due to extended residence time and intricate microstructures. The study reveals that wood type selection in this study, i.e., yellow poplar (*Liriodendron tulipifera*), European beech (*Fagus sylvatica*), Douglas fir (*Pseudotsuga menziesii*), and silver fir (*Abies alba*), plays a crucial role in filtration efficiency, with beech emerging as a high-performing option alongside silver fir. Importantly, the optimal range of size exclusion was identified (160–490 nm), aiding in designing wood filters for specific particle size reduction goals. Wood filters also show great potential for removing a broad range of microorganisms, i.e., bacteria and protozoa, as well as nanoplastics and microplastics, which could have profound implications for water treatment and environmental remediation. Furthermore, the study highlights the adsorption/diffusion process through the amorphous domains of the wood biopolymers, i.e., cellulose, hemicelluloses and lignin, enhanced by electrostatic interactions in the filtration efficiency for small organic molecules, providing valuable insights into filtration mechanisms.

✉ Antoni Sánchez-Ferrer
sanchez@hfm.tum.de

Jenifer Guerrero Parra
jenifer.guerrero@tum.de

[1] School of Life Sciences, Chair of Wood Science, Technical University of Munich, D-80797 Munich, Germany

Published online: 14 March 2025

Introduction

Water covers 70% of the Earth's surface, but only 2.5% is freshwater, and only 0.26% of this freshwater is available for human consumption (Karim et al. 2019). Furthermore, more than a quarter of the global population does not have access to safe drinking water, which leads to health issues like child mortality, the spread of waterborne diseases, and generalized malnutrition (Osseiran & Lufadeju 2019). Microbial contamination of groundwater and surface water can lead to waterborne illnesses (UN-Water 2021), like gastroenteritis, cholera, and typhoid, manifesting dangerous conditions such as diarrhea, vomiting, inflammations, and fever. Therefore, contaminated water is the most serious threat to human health, causing around 505,000 diarrheal deaths per year (World Health Organization, 2023). Some of the most common causal organisms of diarrhea are listed in Table 1 (Ramchander 2016).

Water treatment processes can prevent the spread of waterborne infections. In developed countries, the water supply is typically handled by centralized water treatment facilities. These centralized facilities entail processes such as chlorination, filtration, adsorption, and osmosis, which are essential for removing dangerous pathogens and contaminants (Iwuozor 2019; Sol et al. 2021). Furthermore, these treatment facilities usually require complex piping systems (Pooi and Ng 2018). Therefore, the initial investment costs of centralized water treatment systems and distribution systems are a barrier to their installation in developing countries and rural areas due to the low density of housing and lack of resources. Most of these technologies are rather expensive for most communities and require constant monitoring, rendering the process almost impossible to implement (Cescon and Jiang 2020). In this context, there is an urgent demand for innovative processes that surpass existing technologies. Specifically, the development of cost-effective, easily accessible, highly efficient, disposable membrane materials that can effectively remove pathogens has significant potential to enhance our ability to deliver safe drinking water. This is the case for ceramic and charcoal water filters but with the drawbacks of being too fragile, requiring high energy-intensive steps during production, or containing silver to avoid biofilm formation (Agrawal and Bhalwar 2009; Mdee et al. 2024).

Table 1 Common organisms found in water that cause diarrheal diseases (Ramchander 2016)

Pathogen		Diameter
Viruses	*Rotavirus*	60–80 nm
	Norovirus	23–40 nm
	Hepatitis	20–60 nm
	Astrovirus	28–35 nm
	Enteric adenovirus	25–31 nm
Bacteria	*Diarrheagenic E. coli*	1.1–6.0μm
	Shigella spp.	0.7–1.0μm
	Salmonella enteritidis	0.7–5.0μm
	Campylobacter spp.	0.2–0.8μm
	Vibrio cholerae	0.5–2.6μm
Protozoa	*Entamoeba histolytica*	10–20 μm
	Cryptosporidium parvum	4.0–6.0μm
	Giardi intestinalis	7.0–20 μm
	Cyclospora cayetanensis	7.5–10 μm

Wood, with its high porosity, large internal surface area, and unique structure, can serve as a natural filter, making it an efficient conduit for water able to retain particulate matter (Plötze and Niemz 2011). Wood's diverse range of pore sizes, porosity and capacity to be tailored to specific structural characteristics make it a promising alternative to traditional filtration systems, e.g., ceramic and charcoal water filters. Wood is mechanically more flexible and less fragile than ceramics, has a similar porosity to charcoal - therefore, has the potential to remove pathogens, i.e., bacteria and protozoa -, consumes less energy during production, and is natural, cheap and sustainable. Its intricate composition gives wood exceptional mechanical, transport, and optical properties, particularly at the nanoscale, making it a versatile material for numerous applications (Berglund and Burgert 2018).

One of the first studies on this topic was conducted by Correa and Sens (2002), who found a relationship between wood density and porosity when selecting a particular wood species for water filtration, followed by further studies on how dead-end filtration and helical cross-flow affect the system's ability to filter (Sens et al. 2015). However, investigations of wood-based filtration systems gained prominence in 2014 after Boutilier et al. (2014) demonstrated that the porous tissue in plants that carries water and nutrients might filter bacteria from water through straightforward pressure-driven filtering. They discovered that roughly 3 cm^3 of *Pinus strobus* can filter up to 4 L of water per day (Boutilier et al. 2014). Similar results were obtained by Potash (2016) and Ramchander (2016), although Ramchander achieved a higher flow rate of 212 mL/(h cm^2) by applying a pressure of 69 kPa, compared to Boutilier's flow rate of 57 mL/(h cm^2) which was achieved with 34 kPa pressure (Boutilier et al. 2014). Other studies in the area found that *Pinus kesiya* wood had a similar removal rate and flow rate to *Pinus strobus* for *Escherichia coli* bacteria (Chitaman et al. 2019). Hanief et al. (2021) achieved a successful removal rate of 99.8% for particles larger than 300 nm using *Kashmiri cypress*. *Ginkgo biloba* wood proved to be a highly effective angiosperm at filtering out *Rotavirus* (70 nm) in Ramchander's experiments (2016)(2021), achieving a high flow rate of up to 692 mL/(h cm^2). Hashim et al. (2022) found that *Manihot esculenta* xylem filters showed good rejection rates, filtering 99.9% of *Escherichia coli* at a flow rate of 0.83 mL/(h cm^2). Vitas (2019) tested a xylem filter made from *Fagus sylvatica* to remove two particle sizes of 5 and 20 µm. Beech wood was unable to filter out completely all particles of 5 µm diameter, but surprisingly, it exceeded the researchers' expectations by removing the 20 µm size particles with almost 99% particle retention. Before executing the experiments, Vitas created a model to predict the filtering results, which matched the actual results for 5 µm particles, but underestimated the effectiveness of the beech wood for 20 µm particles by a factor of ten. The author suggested that the increase in rejection rate due to cake layer building requires further investigation. Ansari et al. (2019) tested whether *Saraca asoca* could filter out mud and found that it was effective, outperforming other species such as *Azadirachta indica*, *Psidium guajava*, *Mangifera indica*, and *Grevillea robusta*. *Phyllanthus emblica* bark powder was found to reduce the total hardness of water by Shanthamareen and Wijeyaratne (2018). Sathish et al. (2012) immersed *Phyllanthus emblica* pieces in polluted water to remove *Escherichia coli* bacteria, but the results showed both poor removal rates and taste of the filtered water.

While previous research has examined wood's potential for microfiltration, critical knowledge gaps persist. Thus, this paper systematically compares different wood species and investigates the role of wood's anisotropic properties in wood-based water filtration systems. The objective was to provide valuable insights into the potential of wood as a sustainable and effective solution for water treatment by assessing the efficiency of various xylems in filtering nanoparticles (NPs) and molecules of different sizes and structures, as well as examining the directional properties of wood in the filtration process.

Materials and methods

Wood filters

The wood species selected for all experiments were yellow poplar (*Liriodendron tulipifera*), European beech (*Fagus sylvatica*), Douglas fir (*Pseudotsuga menziesii*), and silver fir (*Abies alba*) with corresponding densities of 400, 750, 530 and 415 kg/m^3, respectively (Drechselholz Laschinger, Germany). Wood filters were obtained by cutting the wood into approximately 60 × 60 mm² pieces with a thickness of 1 mm in the three orthotropic directions, i.e., L, R, and T, for each wood species. The samples were soaked in deionized water at room temperature for one day. Subsequently, they were circularly cut to create filters with a diameter of 50 mm and a thickness of approximately 1 mm (Figure SI-1) and then stored in a controlled climate chamber at 20 °C and 65% relative humidity (WK3, Weiss Umwelttechnik, Germany). All wood filters were immersed in 10 mL of deionized water for one day before any filtration experiment to avoid any volume change.

Nanoparticles

Nanocrystalline cellulose (NCC, CelluForce, Canada), guar gum (GG, Sigma, Germany), iron (III) oxide (Fe_2O_3, Camassia, Spain), silica (SiO_2, Camassia, Spain) and silica microspheres (μ-SiO_2, Camassia, Spain) were selected as tracers due to their stability and for the evaluation of the different wood species and directions as filtration systems. Dispersions of 0.3% concentration were prepared by dispersion in deionized water at pH 7 for NCC and GG, and at pH 12 for Fe_2O_3, SiO_2, and μ-SiO_2, with a high-speed homogenizer (VEVOR FSH-2 A) for up to 5 min. The dispersions were diluted to obtain calibration samples with 1, 10, 30, 100, 300, and 1000 ppm concentrations. Filtration experiments were conducted using dispersions of 100 ppm concentration.

Dyes

Methylene blue (MB; Sigma-Aldrich, Germany), phenolphthalein (PH; Sigma-Aldrich, Germany), and 4-hydroxy-4'-methoxyazobenzene – azobenzene - (AZ; synthesis: Sanchez-Ferrer et al. 2011) were used as dyes for the filtration evaluation of beech wood in the three directions as filtration system. Solutions of 100 ppm in

deionized water (MB at pH 7, PH at pH 4 and 12, and AZ at pH 12) were prepared and used as references for each dye and for the filtration experiments.

Filtration procedure

In a filtration experiment, a wood filter of 50 mm diameter with ca. 1 mm thickness was put in between a 1000 mL filter flask and a 300 mL graduated funnel clamped by the sturdy aluminum clamp with a connection to the water trap followed by the vacuum membrane pump (Figure SI-1). Then, 10 mL of water with a pH value equal to the pH of the tracer dispersion or dye solution to be filtered was added to the graduated funnel to remove extractives or impurities left in the wood filter. Subsequently, 10 mL of a tracer dispersion or dye solution was added to the funnel to run the experiment for each wood species and for the three orthotropic wood directions. The resulting filtered water was collected in the filter flask and ready for analysis.

Dynamic light scattering

Dynamic Light Scattering (DLS) experiments were conducted with a Zetasizer Nano ZS instrument (Malvern Panalytical, UK) to establish the calibration curve for each tracer and to determine the size distribution of the tracer particles, the corresponding hydrodynamic radius, and the concentration after filtering. DLS measurements were performed using a scattering angle of 173° with a helium-neon laser ($\lambda = 633$ nm) as the light source. Disposable semi-micro low-volume (1.5-3 mL) polystyrene cells (VWR, Germany) were used. The suitable parameters, i.e., the water viscosity of $\eta = 1.0016$ mPa·s, the sample temperature of 20 °C, and the refractive index of $n = 1.3317$ for water. Hydrophobic polytetrafluoroethylene (PTFE) syringe filters of 0.45 µm pore size and 13 mm diameter (VWR, Germany) were used for filtering the organic tracers. All samples were measured three times, and an average correlation curve for each sample was constructed for further evaluation and analysis.

By analyzing the decay of the electric field autocorrelation function $g_1(t)$, DLS allows for the calculation of the translational diffusion coefficient (D) of the tracer particles (Berne and Pecora 2000), which is related to their size in terms of hydrodynamic diameter (d_h) (Raval et al. 2019) as shown in Eq. 1.

$$D = \frac{k_B T}{3\pi\,\eta\,d_h} \tag{1}$$

where T is the temperature of the sample, k_B is the Boltzmann constant, and η is the solvent viscosity.

In the case of a monodisperse sample, $g_1(t)$ can be approximated as a single exponential decay function. However, sample dispersions typically exhibit polydispersity. This requires the consideration of multiple exponential decay functions with varying decay rates. In order to address this issue, the cumulative expansion with the Taylor expansion technique (cumulant method) (Mailer et al. 2015) was employed for calculating the diverse parameters derived from the $g_1(t)$ curve for both monodisperse and polydisperse solutions as shown in Eq. 2.

$$g_1(t) = Ge^{-\Gamma t}\left(1 + \frac{\mu_2}{2}t^2 - \frac{\mu_3}{6}t^3\right) + G_0 \quad (2)$$

where Γ, μ_2 and μ_3 describe the average decay rate, variance, and symmetry of the decay rates of the distribution, respectively, and the parameters G and G_0 represent the amplitude and baseline of the fitting curve, respectively.

Commonly, a polydispersity index $PdI = \mu_2/\Gamma^2$ expresses the width of the distribution, and parameters beyond μ_3 are avoided to prevent overfitting the data. Figure SI-2 shows the electric field autocorrelation function $g_1(t)$ for a 300 ppm NCC dispersion and the corresponding analysis after fitting with experimental data with Eq. 2.

After evaluating the decay rate, the diffusion coefficient can be calculated following Eq. 3.

$$D = \frac{\lambda^2\Gamma}{16\pi^2 n^2 sin^2\left(\frac{\theta}{2}\right)} \quad (3)$$

where λ is the laser wavelength, n is the solvent refractive index, and θ is the scattering angle.

This calculation, together with Eq. 1, allows for the evaluation of the average size (d_h) of the tracers (Figure SI-3). The average size for NCC, GG, Fe_2O_3, SiO_2 and μ-SiO_2 determined by DLS was ca. 120, 270, 530, 330, and 420 nm, respectively, at a concentration of 100 ppm.

Moreover, the photon count rate of the detector also provides insights into the sample concentration. Therefore, calibration curves can be constructed for each tracer sample that correlates the photon count rate to the sample concentration (Figure SI-4). In this way, the final concentration of a tracer particle can be determined before and after the filtration process to evaluate the corresponding filtration efficiency (Austin et al. 2020a).

Ultraviolet-visible (UV–Vis) spectrophotometry

UV-Vis spectroscopy experiments were carried out using a UV-2450 Shimadzu spectrophotometer (Shimadzu, Japan) in order to quantify the concentration of absorbing substances in the dye solutions. MB, PH, and AZ solutions exhibited strong colors, with MB appearing as a deep blue color (pH 7), PH displaying a vibrant pink color at pH 12, and azobenzene an intense orange color (pH 12). To ensure precise analysis, each sample's concentration was reduced by a dilution factor of ca. 50, except for PH, which was transparent at pH 4 and, due to the low absorption, there was no need for dilution. UV-Vis quartz cuvettes of 1 cm path length and 3.5 mL volume were used for the measurements at 25 °C.

Scanning electron microscopy

Scanning Electron Microscopy (SEM) images were captured using a Carl Zeiss EVO-40 XVP electron microscope (Carl Zeiss, Germany) to examine the microstructure of each wood species in the three orthotropic orientations and the tracers. In addition,

a secondary detector (Everhart -Thornley detector) was used at a high voltage value between 10 kV and 15 kV. The distance for the SEM image varied between 12 mm and 20 mm. The samples were sputtered with gold in a sputtering unit (PS-2, International Science Instruments) in a vacuum atmosphere at a voltage value of 1.4 kV and 30 mA of intensity.

Molecular simulations

Structures were drawn using HyperChem 8.0.3 software, and the semi-empirical quantum mechanics method Austin Model 1 (AM1), together with the Polak–Ribiere conjugate gradient algorithm with a root-mean-square (RMS) gradient of 0.05 kcal $Å^{-1}$ mol^{-1}, was used for the geometrical optimization of the molecules, as well as the spin-pairing restricted Hartree-Fock (RHF) operators for all neutral species. The self-consistent field (SCF) convergence limit was set at 10^{-5}, and the accelerated convergence procedure was used. All geometrical values and some quantitative structure-activity relationship (QSAR) parameters were obtained from the quantum mechanics simulations.

Results and discussion

Nanoparticles filtration

The use of nanoparticles (NPs) as tracers for the filtration experiments is due to similarities in shape and size to those from bacteria. Therefore, the analysis of the filtration process using NPs – polymeric or inorganic NPs – can give some idea about the capacity of wood for removing objects or certain dimensions below 1 µm.

The arrangement of wood cells is intricately shaped by the conical geometry of trees and the orientation of cutting planes, leading to three principal orthotropic directions: longitudinal (L), radial (R), and tangential (T) direction. These directions exert profound influences on wood's permeability, flow rate, and filtration efficiency (Wiedenhoeft and Eberhardt 2021). In the L-direction, wood shows elongated cells known as tracheids in gymnosperms and vessels - and also the so-called fibers - in angiosperms (Figure SI-5) (Chen et al. 2020). These tracheids and vessels play a dual role in both fluid transportation and structural support (Fackler and Thygesen 2013). Gymnosperm tracheids in the T-direction often feature cross-field pits, whereas angiosperms exhibit vessel-ray pits, enhancing water flow between adjacent cells. In the R-direction, rays, frequently in the form of aggregate or composite rays, are predominantly found in both gymnosperms and angiosperms (Figure SI-5, SI-6 and SI-7).

To understand the practical implications of these wood cell arrangements, water filtration experiments were conducted using two angiosperm and two gymnosperm species. The wood specimens were cut in the three orthotropic directions, i.e., L-, R- and T-direction. This approach allowed us to explore the filtration capabilities of each direction and gain insights into how the arrangement of cells and the orientation

of these orthotropic directions influence the filtration efficiency of wood-based water filtration systems.

First experiments were performed using iron (III) oxide (Fe_2O_3) nanoparticles due to their good visibility. Figure 1 shows the filtrates after passing through wood disks of ca. 1 mm in thickness in the three directions for the four wood species, together with the filtrate concentration evaluated via DLS.

From the deep-red Fe_2O_3 reference dispersion (105 ppm), it can clearly be observed that filtrates appear visually clearer in both the R- and T-direction with filtration efficiency values ranging from 98 to 99.9% concentration reduction – except for Douglas fir in the T-direction (86%) and poplar in the R-direction (71%) –, while the filtrate concertation in the L-direction looks reddish and with filtration efficiency values from 47 to 75%. These results suggest that the anatomical differences between wood species and wood directions play a major role when filtering nanoparticles, especially in the R- and T-direction.

Wood species are categorized into gymnosperms (coniferous trees) and angiosperms (flowering trees), with gymnosperms characterized by a tissue primarily composed of tracheids, which are imperforate elements with bordered pits. Notably, gymnosperms lack vessels, as the fluid transport takes place in the longitudinal tracheids. These tracheids vary in diameter from 10 to 80 µm. In contrast, angiosperms feature vessels with a broader diameter range of 17 to 500 µm, together with fibers meant for structural purposes. The interconnections between vessels or tra-

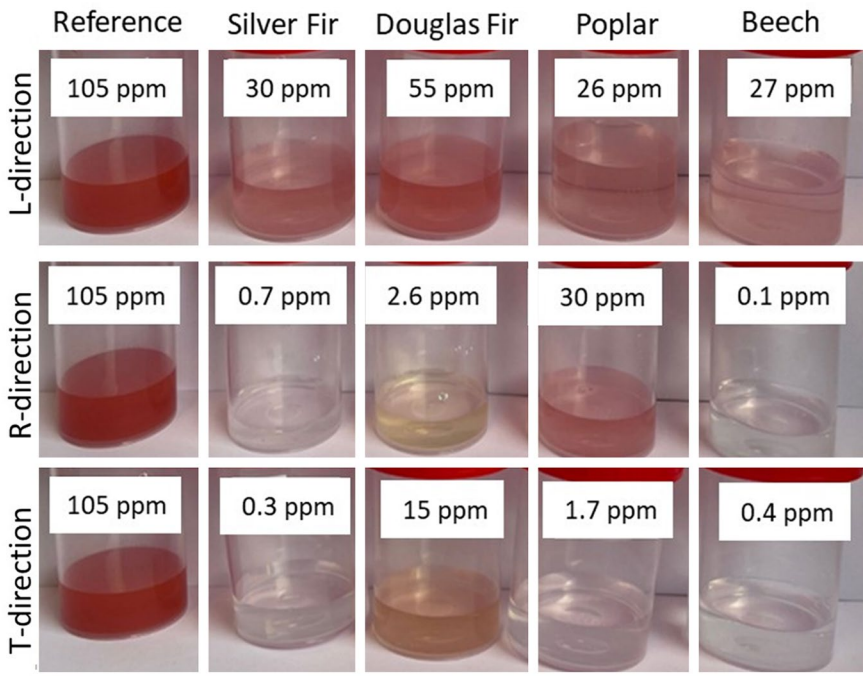

Fig. 1 Fe_2O_3 NP dispersion samples (initial concentration 105 ppm) – collected after filtration through 1 mm wood disks. Results of four wood species (columns) in the three wood directions (rows)

cheids are called pits, equipped with membranes, or margos, that control the flow of water through the tree. The pore size of these margos varies among tree species, typically ranging from 100 to 500 nm in gymnosperms (Choat et al. 2008) and about 70 to 500 nm in angiosperms (Jansen et al. 2009). Moreover, in the radial direction, both gymnosperms and angiosperms feature some channels called rays, which are in charge of transporting water and storing food.

Wood SEM inspections in the three directions (Figure SI-6 and Si-7) – together with a rough evaluation of mean diameter for the different anatomical features (Table SI-1) – show values of ca. 30–60 µm and 70–150 µm for the tracheids and vessels diameter, respectively (Sperry et al. 2006), while rays and pits diameter values range from 8 to 18 µm (Ruffinatto et al. 2023) and 2 to 8 µm (Choat et al. 2008), respectively. The mean diameter values for poplar (up to 8 µm) and Douglas fir (up to 18 µm) for the respective R- and T-direction could be correlated to the lower filtration efficiency of 86% and 71%, respectively.

The big difference between the R/T-directions and the L-direction filtration efficiency is directly connected to the mean diameter values of the wood natural filtration channels or lumina (Sperry 2003). This geometrical factor has a direct effect on the residence time for the nanoparticles and on the flow rate values during the filtration process. In the L-direction, the flow rate is in the range of 550 to 600 mL/(h cm^2), while in the other two directions falls between 0.01 and 0.40 mL/(h cm^2), showing differences of 3 to 4 orders of magnitude higher for the L-direction (Table SI-2).

After the preliminary experiments with Fe_2O_3 NPs, filtration experiments were performed with the corresponding DLS analysis with the rest of the NPs of polymeric or inorganic nature in order to observe the particle removal and size exclusion effect from wood as a function of the size, nature, and shape of the tracers, the wood species and the filtration direction.

DLS experiments were performed to evaluate the hydrodynamic diameter (d_h) and the polydispersity index (PdI), as well as the concentration of NPs, before and after filtration. In total, five different nanoparticles were studied as tracers: nanocellulose (NCC: negatively charged needle-like and rigid particles), guar gum (GG: neutral, spherical and deformable particles), iron (III) oxide (Fe_2O_3: negatively charged and rigid particles), silica (SiO_2: negatively charged and rigid particles), and silica microspheres (µ-SiO_2: negatively charged and rigid particles). The d_H (and PdI) values for the NNC, GG, Fe_2O_3, SiO_2 and µ-SiO_2 NPs were 130 nm (0.35), 435 nm (0.21), 506 nm (0.15), 282 nm (0.31), and 606 nm (0.85), respectively, with some aggregates or bigger particles in the micron scale (Figure SI-8). Dispersions of ca. 100 ppm in concentration were filtered in the three wood directions for each wood species and the filtrates were analyzed by DLS (Figure SI-9, SI-10, SI-11, SI-12 and SI-13). The resulting hydrodynamic diameter d_h before and after filtration (Fig. 2), along with the corresponding particle size reduction percentage, are reported in Table 2 for each wood species, i.e., silver fir, Douglas fir, poplar, and beech, and for the three directions, i.e., L, R and T.

The outcomes of the analysis indicate a notable size reduction in NPs with diameters exceeding approximately 200 nm. In this sense, NCC shows minimal size exclusion in any of the three directions for all wood species with d_h values around 112–130 nm (maximum of 14% in size reduction), and as shown in the PSD profiles

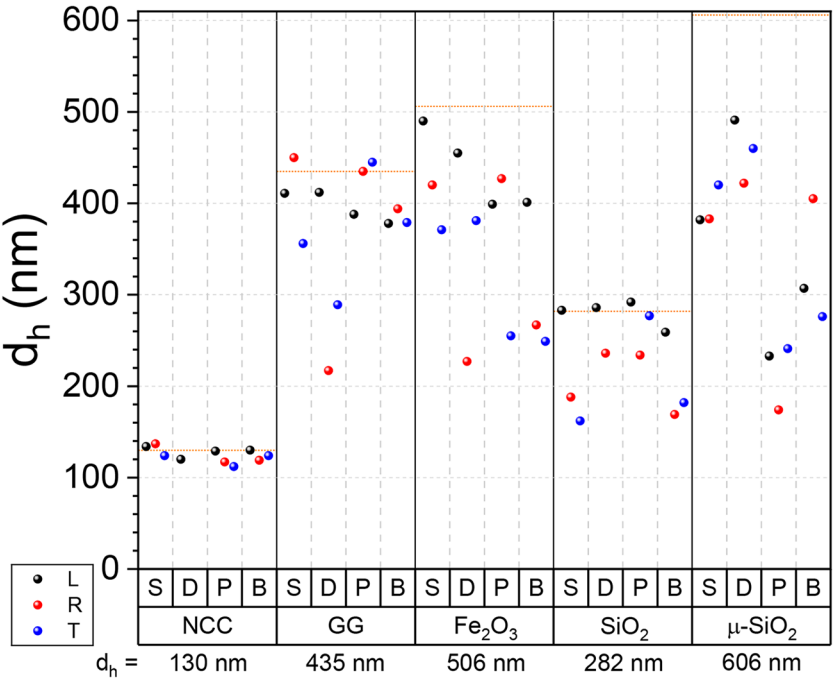

Fig. 2 Hydrodynamic diameter of the NPs (NCC, GG, Fe_2O_3, SiO_2 and μ-SiO_2) in the filtrates after filtration in the three directions (L, R and T) for the four wood species (S = silver fir, D = Douglas fir, P = poplar, and B = beech). The orange dotted lines are the hydrodynamic diameter values for each tracer before filtration

Table 2 Hydrodynamic diameter d_h for each tracer after filtration for the four wood species and the three directions (L, R and T) together with the corresponding particle size reduction percentage in parenthesis. The hydrodynamic diameter before filtration for NNC, GG, Fe_2O_3, SiO_2 and μ-SiO_2 was 130, 435, 506, 282 and 606 nm, respectively

Wood	Direction	d_h (nm)				
		NCC	GG	Fe_2O_3	SiO_2	μ-SiO_2
Silver fir	L	134 (0%)	411 (6%)	490 (3%)	283 (0%)	382 (37%)
	R	137 (0%)	318 (27%)	420 (17%)	188 (33%)	383 (37%)
	T	124 (5%)	356 (18%)	371 (27%)	162 (42%)	420 (31%)
Douglas fir	L	120 (7%)	412 (5%)	455 (10%)	286 (0%)	491 (19%)
	R	nd	217 (50%)	227 (55%)	236 (16%)	422 (30%)
	T	nd	289 (34%)	381 (25%)	nd	460 (24%)
Poplar	L	129 (1%)	388 (11%)	399 (21%)	292 (0%)	233 (62%)
	R	117 (10%)	435 (0%)	427 (16%)	234 (17%)	174 (71%)
	T	112 (14%)	445 (0%)	255 (50%)	277 (1%)	241 (60%)
Beech	L	130 (0%)	378 (13%)	401 (21%)	259 (8%)	308 (49%)
	R	119 (9%)	394 (10%)	267 (47%)	169 (40%)	405 (33%)
	T	124 (5%)	379 (13%)	249 (51%)	182 (35%)	276 (54%)

(Figure SI-14). GG experiences a slight decrease in size – especially for gymnosperms in the R- and T-direction – with a maximum size reduction of 34-50% for Douglas fir.

Inorganic NPs, i.e., Fe_2O_3, SiO_2 and µ-SiO_2, underwent significant size reduction, particularly in the R- and T-direction. However, the L-direction appears less effective in size exclusion for Fe_2O_3 and SiO_2.

NPs. On the contrary, µ-SiO_2 tracers reveal size exclusion in all three directions, signifying the wood filters' efficiency in excluding particles larger than the size of µ-SiO_2.

The analysis of µ-SiO_2 NPs indicates the presence of two populations within these particles: a nanoparticle distribution centered at 606 nm (PdI = 0.85) and a microparticle distribution at 19 mm (PdI = 0.33). The intensity distribution analysis reveals a percentage of 38% for the NPs, while the analysis of the mass/volume and number distribution renders a presence of 69% and 89%, respectively. DLS analysis is based on scattering intensity and intensity populations are 10^3 times the mass/volume of particles, respectively. After filtration, the 606 nm NP distribution is partially filtered and the 19 µm microparticles (31% in mass/volume) are basically retained.

The filtration efficiency was evaluated based on the final concentration of the tracer with respect to the reference dispersion. In Table 3, the filtrate NP concentration and the corresponding concentration reduction percentage or filtration efficiency are reported for each NP as a function of the wood species and filtration direction, together with the filtration efficiency values that are plotted in Fig. 3. The corresponding NPs removal values expressed in mg/g of wood for each tracer and for the four wood species and the three directions (L, R and T) are summarized in Table SI-3.

NCC shows almost no retention due to its needle-like nature, which makes it easy to pass through the filter under flow when applying a vacuum, as shown in the corresponding PSD analysis (Figure SI-14), where the intensity and the distribution remain almost the same for all analyzed samples. The 130 nm NCC hydrodynamic

Table 3 Concentration C for each tracer after filtration for the four wood species and the three directions (L, R and T) together with the corresponding concentration reduction percentage or filtration efficiency in parenthesis. The concentration before filtration for NNC, GG, Fe_2O_3, SiO_2 and µ-SiO_2 was 130, 104, 105, 100 and 115 Ppm, respectively

Wood	Direction	C (ppm)				
		NCC	GG	Fe_2O_3	SiO_2	µ-SiO_2
Silver fir	L	140 (0%)	65 (37%)	30 (71%)	94 (6%)	16 (86%)
	R	184 (0%)	62 (40%)	**0.7 (99.3%)**	65 (35%)	19 (84%)
	T	145 (0%)	68 (35%)	**0.3 (99.7%)**	42 (58%)	22 (81%)
Douglas fir	L	131 (0%)	83 (20%)	55 (47%)	87 (13%)	27 (76%)
	R	nd	173 (0%)	2.6 (98%)	76 (24%)	16 (86%)
	T	nd	363 (0%)	15 (86%)	nd	15 (87%)
Poplar	L	143 (0%)	68 (35%)	26 (75%)	96 (4%)	8.5 (93%)
	R	130 (0%)	96 (7%)	30 (71%)	107 (0%)	8.6 (93%)
	T	98 (25%)	67 (35%)	1.7 (98%)	96 (4%)	8.8 (92%)
Beech	L	135 (0%)	63 (40%)	26 (75%)	92 (8%)	14 (88%)
	R	119 (9%)	48 (54%)	**0.1 (99.9%)**	45 (55%)	19 (83%)
	T	149 (0%)	89 (14%)	**0.4 (99.7%)**	67 (33%)	15 (87%)

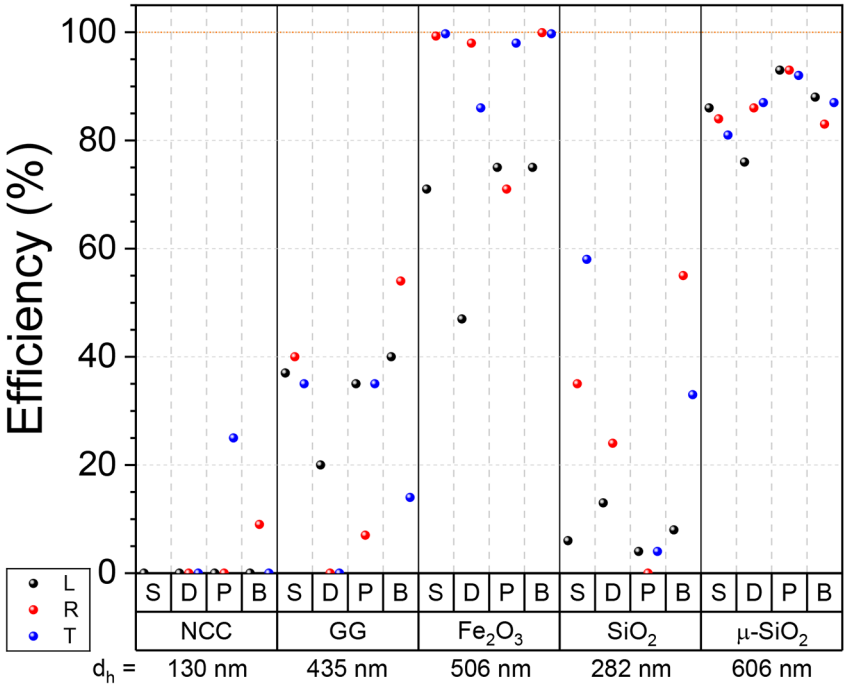

Fig. 3 Filtration efficiency for the four wood species (S = silver fir, D = Douglas fir, P = poplar, B = beech) in the three directions (L, R and T) for the five NPs (NCC, GG, Fe_2O_3, SiO_2 and μ-SiO_2) after filtration. The orange dotted line corresponds to 100% efficiency

diameter corresponds well to particles of average length of *ca.* 220 nm and anaverage diameter of *ca.* 35 nm (Londoño et al. 2018). GG shows amodest filtration efficiency with maximum values around 40%, which is explained by the deformability of this 435 nm polymeric NP. The PSD analysis (Figure SI-15) indicates a decrease in the intensity and a shift of the distributions towards lower size values that confirm the partial removal of the NPs with little size exclusion. The 506 nm Fe_2O_3 NPs reached morethan 99% of filtration efficiency for silver fir and beech in the R- and T-direction and around 70-75% in the L-direction. The corresponding PSD analysis clearly indicates a huge decrease in the intensity of the distributions as a result of the retention of these Fe_2O_3 NPs (Figure SI-16). The 282 nm SiO_2 NPs were partially filtered outwith efficiency values around 10% in the L-direction and around 30-50% in the R- and T-direction. This retention is similar to the one from the 435 nm GG particles as shown by a decrease in the PSD intensity after filtration (Figure SI-17). The bimodal 606 nm/19 mm m-SiO_2 particles show a significant filtration performance with an 80-90% efficiency. While the 19 mm microparticles are completely removed, the 606 nm NPs greatly decreased in intensity, as shown in the corresponding PSD analysis when comparing the original dispersion with the filtrates (Figure SI-18).

The results indicate that wood filters significantly reduce particle sizes, primarily in the range of 160 nm to 490 nm – minimum and maximum d_h values, respectively - for the inorganic NPs studied. This range is a crucial parameter for understanding

wood filter performance in terms of size exclusion. A complete map for the NP size reduction and polydispersity index is shown in the Supporting Information (Figure SI-19 and SI-20).

The microstructural characteristics of wood species play a pivotal role in filtration efficiency. The arrangement of cells, the presence of vessel elements, and the density of fiber networks all influence how effectively wood filters reduce the particles' concentration and size. Based on the excellent results from silver fir and beech in the R- and T-direction (99.3–99.9% efficiency), it can be concluded that the most relevant anatomical features in wood are the pits that work as a bottleneck in the filtration process (Choat et al. 2008). That is the case for silver fir and beech with minor/major pit diameters values of 4/5 and 2/5 µm when filtering a 506 nm Fe_2O_3 NP dispersion. Therefore, the filtration process' complexity underscores the critical role of the physical attributes of the filtration medium in its efficacy.

As a practical example, beech wood cylinders of 4.5 mm in length and 2.5 mm in diameter were prepared, allowing for the filtration in the L-direction. The wood filter was swollen and inserted into a commercial pump water filter system (Figure SI-21 A). The 100 ppm Fe_2O_3 NP dispersion and 1000 ppm µ-SiO_2 particle dispersion were filtered using this technique with a final concentration of ca. 10 ppm in Fe_2O_3 and ca. 5 ppm in µ-SiO_2 NPs, respectively (Figure SI-21B and SI-21 C). The filtration process for both samples is available as videos in the Supporting Information (Video SI-1 and SI-2), showing that a portable, manual, and economical filtration procedure can easily be implemented.

Because the flow rate in the R/T-directions is rather low, the thickness of the discs can be optimized for achieving high removal rates. As an example, increasing the thickness of silver fir, Douglas fir, poplar, or beech wood filters in the L-direction from 1 mm to 3.72 mm, 7.25 mm, 3.32 mm and 3.32 mm, respectively, a 99% removal of Fe_2O_3 NPs can be achieved with flow rates of 550–600 mL/(h cm^2). In this spirit, the penetration depth L for each inorganic NP and wood species can be estimated based on the filtration efficiency values obtained for the 1 mm thickness filters (Table 4) by applying the exponential decay $\eta = 1\text{-}\exp(-t/L)$, where η is the filtration efficiency and t is the thickness of the sample.

From the values in Table 4, it is evident that the small NPs, i.e., SiO_2, have larger penetration depth values and, therefore, need thicker wood filters than big NPs, i.e., Fe_2O_3 and µ-SiO_2. This effect is shown in Fig. 4, where the filtration efficiency is plotted as a function of the thickness of the sample allowing to estimate the thickness value for a certain removal efficiency for each wood species and inorganic NP.

From Fig. 4, the grouping of the curves by NPs diameter is shown, where µ-SiO_2 NPs (d_h = 606 nm) have thickness values to achieve 99% filtration efficiency between 1.73 mm and 3.23 mm, Fe_2O_3 NPs (d_h = 506 nm) between 3.32 mm and 7.25 mm, and SiO_2 NPs (d_h = 282 nm) between 33.1 mm and 113 mm. Therefore, an optimized

Table 4 Penetration depth values L for the four wood species and the three inorganic NPs, i.e., SiO_2, Fe_2O_3 and µ-SiO_2

NPs	d_h (nm)	L (mm)			
		silver fir	Douglas fir	poplar	beech
SiO_2	282	16.2	7.18	24.5	12.0
Fe_2O_3	506	0.808	1.58	0.721	0.721
µ-SiO_2	606	0.509	0.701	0.376	0.472

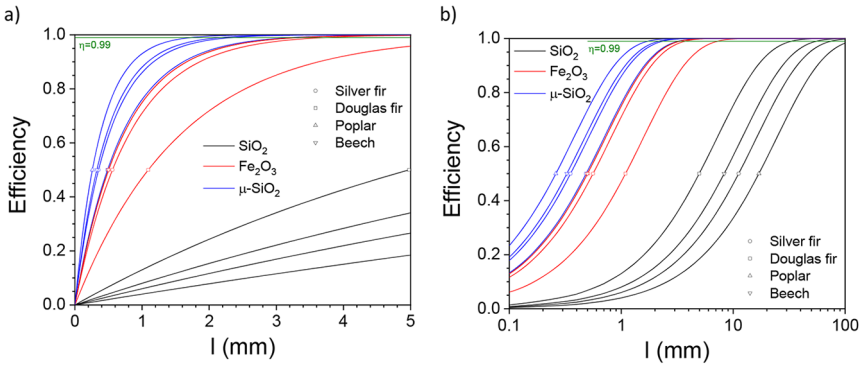

Fig. 4 Filtration efficiency as a function of the thickness for each wood species and for the three inorganic NPs, i.e., SiO_2 (black), Fe_2O_3 (red) and μ-SiO_2 (blue) in (**a**) lin-lin and (**b**) log-lin scales. The green line corresponds to the 99% filtration efficiency

thickness could be estimated for each wood species to successfully filter NPs of a certain diameter.

Dyes filtration

After determining the optimal wood species and filtration direction from all wood-based filtration systems, further tests with dyes (Selim and Mohamed 2017) were conducted, focusing specifically on the beech wood filters due to the good performance shown with nanoparticles. Such dyes, i.e., methylene blue (MB), azobenzene (AZ), and phenolphthalein (PH), are small molecules with molar mass values around 220 to 320 Da and with the largest dimension between 1.0 and 1.4 nm (Figure SI-22). Therefore, the removal of such compounds by filtration with wood could only be due to electrostatic interactions or other kinds of weak interactions. To evaluate the filtrate's effectiveness in dye removal, UV-Vis spectroscopy analysis was performed. MB - a flat and positively charged molecule (pH 7) -, AZ - a flat and negatively charged compound (pH 12), and PH - an almost spherical, neutral (pH 4) or negatively charged (pH 12) molecule – show maximum absorption wavelength values at λ_{max} = 664, 436, 276 and 553 nm (Figure SI-23).

In Fig. 5, the UV-vis spectrum for each dye at 100 ppm concentration is shown together with the corresponding spectrum after filtration across all three directions, i.e., L, R and T. In all cases, the removal of the dyes occurred in all directions with a slightly better performance in the R- and T-direction, as observed by the decrease in the corresponding peak maxima. Notably, the filtration efficiency of MB was higher compared to the other dyes in all three directions. This can be attributed to the cationic nature of this dye, which can interact with the negatively charged groups in some hemicelluloses in the wood cell wall, while the neutral or anionic dyes are retained due to weak interactions with the wood bio-polymers, e.g., hydrogen bonding, π-π interactions and dispersion forces (Pimentel et al. 2023), once the dyes are adsorbed and diffuse through the wood cell wall.

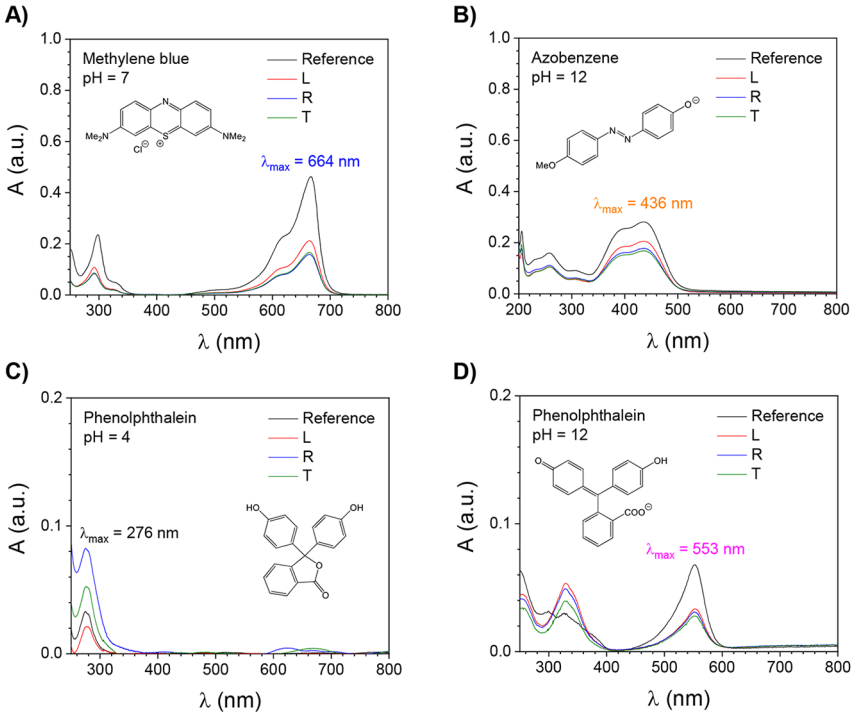

Fig. 5 UV-Vis spectra of dye solutions (100 ppm) before (reference) and after filtration in the L-, R- and T-direction using beech as a filter: **A**) methylene blue at pH 7, **B**) azobenzene at pH 12, **C**) phenolphthalein at pH 4, and **D**) phenolphthalein at pH 12

Molecular simulations have been performed using the semi-empirical quantum mechanics method Austin Model 1 (AM1) to identify the charge density, molecular volume, excluded volume, dipole moment, radius of gyration, and molecular distances (Figure Si-22). All molecules show a molecular volume and excluded volume values below 0.3 nm^3 and 0.9 nm^3, respectively. These values correspond to a water cluster of 12 to 17 water molecules that are easily present in the amorphous domains of the wood cell wall in the swollen state – hydrogel state. Therefore, the solvated molecules can travel to the cell wall surface, be adsorbed, and diffuse through the amorphous wood domains no matter their size – quite similar and of $V \approx 0.3$ nm^3 – and their shape – flat or bulky molecules.

The present findings provide evidence supporting the operation of the filtration system through a combination of surface interaction and adsorption/diffusion processes (Alfrey 1965). Therefore, the electrostatic interactions between the positively charged MB and the negatively charged components in the wood cell wall interface enhance the already natural filtration process. The main filtration process involves the adsorption of the water-solvated dye molecule on the lumen/cell wall interface, followed by the diffusion of the dye through the cell wall. All these results are summarized in Fig. 6, where the filtration efficiency of beech filters in the three directions is plotted for each dye molecule.

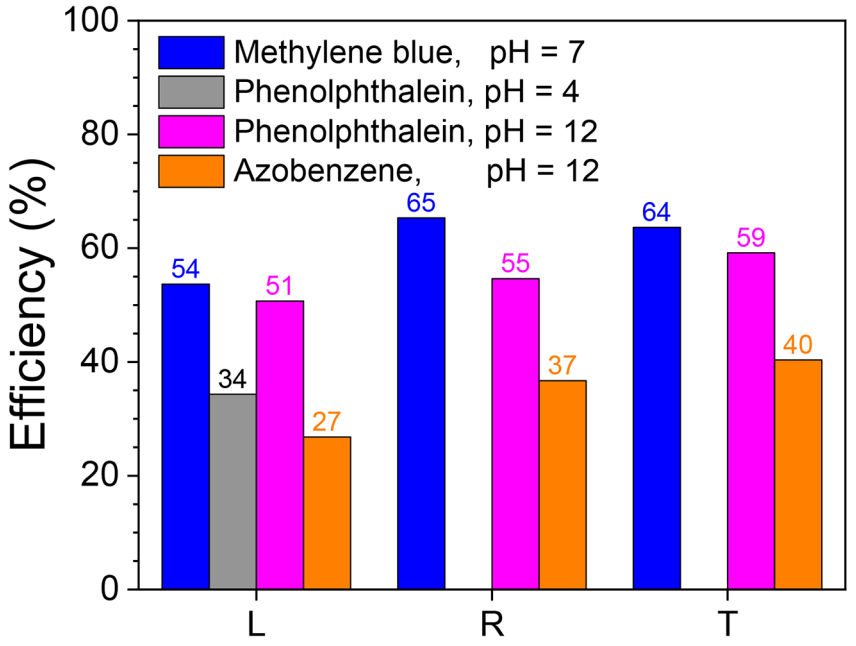

Fig. 6 Filtration efficiency of beech wood with the different dyes in the L-, R- and T-direction

It has to be noticed that the filtration efficiency of the PH filtrate (pH 4) in the R- and T-direction could not be determined because the peak maxima exceeded the intensity of the reference spectrum. A plausible explanation is due to the presence of the primary lignin or lignans that absorb in the UV region, which typically occurs around 280 nm (Fackler and Thygesen 2013). Moreover, these filtrates showed absorption peaks in the 600–700 nm region, pointing out that at this pH, some compounds have been removed from the wood structure. Because the flow rate is 3 to 4 orders of magnitude lower than in the L-direction, the extended filtration time allows for greater extraction of water-soluble lignin/lignans from the wood, leading to deviations from accurate data in the UV region.

However, when subjected to filtration through a beech wood filter, the filtration efficiency for MB, PH at pH 4 and pH 12, and AZ is 54–65%, 34%, 51–59%, and 27–40%, respectively, indicating that small organic molecules (ca. 0.3 nm^3 in volume) can be absorbed in the amorphous domains of the cell wall structure, i.e., cellulose, hemicelluloses and lignin, depending on factors like the nature of the charge, shape and size (Stjepanović et al. 2021).

The difference in removal efficiency between a positively charged molecule like MB and a negatively charged molecule like AZ at pH 12 is between 24% and 28% which could be explained by the interactions of the former with negative charges in the hemicellulose domains. When comparing the results to the negatively charged PH at pH 12, then the hydrogen bonding capabilities of this molecule can bring an extra contribution to be better retained compared to the negatively charged AZ at pH 12, with almost no hydrogen bonding capabilities. This results in a difference in the removal efficiency for PH at pH 12 between 3% and 10% with respect to the posi-

tively charged MB molecule. Finally, the neutral PH at pH 4 has fewer chances for interactions compared to its negatively charged counterpart PH (at pH 12) as seen by a difference in the removal efficiency of 17%.

Therefore, the analysis and testing of a wood-based filtration revealed that the filtration process involves both surface interactions – small cell wall pores – and adsorption/diffusion processes being the last one the most relevant factor. Molecular features like the nature of the charge – neutral, positive or negative charges –, the capability to establish hydrogen bonds, the molecular shape – flat or bulky molecules –, and the molecular size/volume might play a role in the retention of such compounds within the wood structure enhancing the tendency for strong interactions or increasing the number of interactions sites, and resulting in variations in the filtration efficiency.

Comparison with existing household water treatment technologies

The most commonly used low-cost household water treatment technologies (point-of-use, POU) in developing countries are (i) chemical treatment - chlorination and flocculation -, (ii) thermal treatment - solar disinfection -, and (iii) filtration - bio-sand, ceramics and activated charcoal (Lantagne et al. 2006). Because this work aims to find whether wood could be a solution for water treatment based on performance, cost and sustainability, in the following paragraphs, only technologies with local production or ready to be produced locally will be considered keeping in mind that membrane filtration is considered the most effective and least expensive among purification techniques (Aziz et al. 2024). Moreover, a very important point to be considered for the selection of these technologies is the low-income rural context in developing countries (Venkatesha et al. 2020).

Chemical treatment with hypochlorite, e.g., NaClO or $Ca(ClO)_2$, is very efficient for bacteria and protozoa removal (>5 log removal for 50 mg/L concentration) but needs a chlorination plant on site to be cost-efficient (Clayton et al. 2021). It is more efficient when combined with the use of flocculants, e.g., $Al_2(SO_4)_3$, $Fe_2(SO_4)_3$ and $FeCl_3$, which are produced somewhere in developing countries. This water treatment is not very efficient for water contaminated with small organic molecules and some ions due to side reactions with the hypochlorite (Sobsey et al. 2008; Khan and Khan 1984).

Solar disinfection or solar pasteurization is a very efficient technology in removing bacteria (2–5 log removal) but not too much against protozoa (1 log removal). It requires a big surface installation with large amounts of intact and clean plastic bottles that degrade over time. This technology depends on the weather conditions – exposure to the sunlight - in order to achieve enough temperature inside the containers, e.g., 60 °C, to inactivate microorganisms in the water (McGuigan et al. 1999).

Filtration systems are good alternatives to the previous treatments, e.g., bio-sand filtration, ceramic filtration, and biochar, which are relatively economical options and available for the population. Bio-sand filtration is the least efficient of the filtration options (3 log removal for protozoa, and 2 log removal for bacteria). It requires a plastic, metal or concrete container filled with local gravel at the bottom and local fine sand on top. The installation works with a biofilm formation on top of the sand

layer and is responsible for inactivating microorganisms (Kabir et al. 2016). Ceramic filtration is very efficient against bacteria and protozoa (3 log removal) when combined with colloidal silver in the formulation. It is high energy-demanding for production, it needs intensive maintenance to avoid clogging of the pores and it is quite fragile (Soppe et al. 2015). Biochar is also quite efficient against microorganisms (3 log removal) and due to its meso- and nanoporous nature also adsorbs small organic molecules. It requires dry local biomass and a lot of energy for its production via carbonization. Due to the formation of a biofilm during filtration use, biochar granulates or filters must be replaced often (Gwenzi et al. 2017).

All these technologies are optimal when the partners/producers are local, and provide 2.5 to 3 L per person per day (ca. 1 m^3/year). Generally, filtration technologies need maintenance due to recontamination or clogging, replacement of components, and training/education for the users in order to be efficient (UNICEF 2020). The success of these water treatment technologies depends on the local availability and reduced cost of materials to provide a long-term sustainable solution for water filtration. The 5-member family per month cost for chlorination is 0.03–0.07 USD (https://supply.unicef.org/s0000589.html), for chlorination-flocculation is 1.74 USD (https://supply.unicef.org/s5007321.html), for solar disinfection is 0.11 USD (https://www.engineeringforchange.org/), for bio-sand filtration is 0.22 USD (https://www.hwts.info/), for ceramics is 0.69 USD (https://spouts.org/), and for biochar filters is 0.30 USD (https://seasoilfj.com/).

The use of wood as a filtration technology for membrane gravity filters, membrane pumping filters, or screw-cap membrane filters has the advantage of being a local and cheap material that is available in almost all rural areas (Boutilier et al. 2014; Ahmad Ansari et al. 2019) with an estimated but not optimized cost of 1.47 USD per family per month (Ibrahim et al. 2022). Polysulfone hollow fiber membranes for gravity, pumping, or screw-cap filters result in a cost per 5-member family per month of 0.87 USD (https://uzimafilters.org/), 0.73 USD (https://cjh.shop/Marken/Lifesaver/), and 3.13 USD (https://faircap.org/), respectively, but this technology has to be imported from developed countries. Therefore, replacing the expensive synthetic fiber membranes with wood cylinders is a good alternative. As an example, a screw-cap system (2000 L, 0.009 USD/L; https://naturbummler.de/) and a pumping system (5000 L, 0.017 USD/L; https://www.wasserfilter-experten.de/) were used by using ca. 26 cm^3 cylindrical wood filters (27 mm in diameter and 45 mm in height). The estimated cost for silver fir and beech wood filters is around 0.0046 and 0.0050 USD, respectively (180 USD/m^3 and 193 USD/m^3, respectively, with an 80% yield after cutting and debarking; https://www.lesprom.com/). That corresponds to a cost of 0.0009 USD/L to 0.0010 USD/L for 5 L filtered water or 0.35–0.45 USD for a 5-member family per month based on European log prices – affordable and comparable to the water treatment technologies discussed above.

An estimation for the cost of a wood filter used in this work of 50 mm in diameter and 1 mm in thickness, was conducted for the four wood species considering the prices for $60 \times 60 \times 300$ mm^3 pieces from the wood supplier ranging from 2.96 USD to 3.72 USD. Assuming that only 150 filters of 1 mm thickness can be obtained for each 300 mm length piece, the cost is around 0.02–0.03 USD for each wood filter. This filter cost would be much lower when using wood from local European forests

and acquiring huge amounts, e.g., 0.0007–0.0008 USD per filter from 1 m^3 of beech wood (Ahmed and Sánchez-Ferrer 2025), resulting in a final cost of 0.28–0.34 USD for a 5-member family per month based on European log prices. Therefore, despite no tests being conducted for the removal performance of microorganisms, great removal efficiency values are expected against protozoa and ca. 3–4 log removal for bacteria when using 3 cm^3 of wood per person per day (Boutilier et al. 2014). This corresponds to 90 cm^3 of wood per person per month or 450 cm^3 per 5-member family per month. On top of that, these wood filters could be disposed of or burnt but also recused by backwashing them to remove reversible fouling, making wood filters a more economical and sustainable option for water filtration treatment (Pooi and Ng 2018).

Although wood microfiltration, as well as ceramics and biochar, suffers from clogging due to the presence of suspended solids and organic matter, it is recommended to use it combined with a coarse removal technique prior to filtration, e.g., sand filtration or sedimentation. Wood microfiltration can also be used as a cheap pretreatment step to avoid fouling during ultrafiltration, nanofiltration, or reverse osmosis (Gwenaelle et al. 2017). Finally, the use of wood from local forests - a sustainable resource that is easy to obtain and reuse - will help the development of rural areas by creating more jobs and supporting the local economy.

Conclusion

The findings of this study highlight the considerable potential of wood filters in particle removal, size exclusion, and molecular adsorption, offering valuable insights into their performance under various conditions and directional orientations. Notably, wood filters exhibited superior particle removal capabilities in the radial (R) and tangential (T) direction, attributed to their extended residence time and intricate microstructure. The main wood anatomical features that control the removal of particles are mainly pits whose aperture – from 2 to 8 µm – and internal structure are in the range of the size the NPs used as tracers. Moreover, the study revealed that the degree of size exclusion achieved through wood filtration varies based on tracer nature, with NCC and GG showing limited size exclusion due to the needle-like shape and deformability under flow conditions, respectively, while inorganic particles like Fe_2O_3, SiO_2, and µ-SiO_2 demonstrated substantial size exclusion, underscoring the size-dependent sieving behavior of wood filters.

The choice of wood type emerged as a critical determinant of filtration efficiency, with beech wood consistently delivering excellent results for the removal of nanoparticles in the R- and T-direction (99.7–99.9%), along with silver fir (99.3–99.7%), due to the pits' minor/major diameter values of 2/5 µm for beech and 4/5 µm for silver fir. However, practical considerations favored beech wood due to its higher flow rate. This research also identified an optimal size exclusion range of approximately 230–490 nm in the longitudinal direction and 160–460 nm in the radial and tangential directions, providing valuable guidance for designing customized wood filters for specific particle size reduction goals. Importantly, the implications of wood filtration extend beyond particulate matter removal, as this study suggests wood fil-

ters have the potential to remove bacteria and protozoa, as well as nanoplastics and microplastics, within a range from 200 nm to 20 µm, offering significant promise for applications in water treatment and environmental remediation.

Electrostatic interactions were found to enhance the filtration efficiency of small dye organic molecules of ca. 0.3 nm^3 in volume by wood filters. Generally, all water-soluble molecules show adsorption in the lumen/cell wall interface with a diffusion process through the amorphous domains of the wood biopolymers, i.e., cellulose, hemicellulose and lignin. On top of that, a positive charge on the dye molecules, coupled with the negative charge of wood components, led to an improvement in the filtration performance, shedding light on the underlying mechanisms for small molecule filtration processes.

Therefore, wood can be used for filtration processes as a sustainable solution when high-technology products and applications are not available or scarce. The estimated cost for a 5-member family per month is 0.28–0.34 USD based on European log prices with a good performance for microorganism removal based on the NPs used as a model in this study.

Future work will deal with the lumina surface modification with functionalized molecules/polymers in order to narrow the anatomical features of the intrinsic wood structure and to interact selectively with the pathogens and pollutants present in residual or contaminated water. In this regard, wood could be used as a scaffold for the production of microfiltration (nanoparticles, bacteria, protozoa, nanoplastics and microplastics), ultrafiltration (proteins, viruses and colloids), and nanofiltration (organic molecules and ions) systems, e.g., protein purification and ion exchange membranes.

Supplementary Information The online version contains supplementary material available at https://doi.org/10.1007/s00226-025-01645-7.

Acknowledgements The authors thank Anja Vieler for her help in obtaining the SEM images.

Author contributions A.S.F. contributed to the study's conception and design. Material preparation and data collection were performed by A.S.F. and J.G.P. Data analysis was performed by A.S.F. and J.G.P. Figures and tables were created by A.S.F. and J.G.P. The first draft of the manuscript was written by J.G.P. and A.S.F., and both authors commented on previous versions of the manuscript. All authors read and approved the final manuscript.

Funding Open Access funding enabled and organized by Projekt DEAL.
No funding was received for conducting this study.

Data availability No datasets were generated or analysed during the current study.

Declarations

Ethics approval and consent to participate Not applicable.

Consent for publication Not applicable.

Competing interests The authors declare no competing interests.

References

Agrawal VK, Bhalwar BR (2009) Household water purification: Low-Cost interventions. Med J Armed Forces India 65:260–263. https://doi.org/10.1016/S0377-1237(09)80019-1

Ahmad Ansari M, Mustafa S, Husain T, Ali R (2019) Water filtration using plant xylem in Northern India. IOP Conf Ser: Mater Sci Eng 691:012037. https://doi.org/10.1088/1757-899X/691/1/012037

Ahmed MJ, Sánchez-Ferrer A (2025) Wood-supported cationic polyelectrolyte membranes from a reactive ionic liquid for water detoxification. Chem Eng J 505:158841. https://doi.org/10.1016/j.cej.2024.158841

Alfrey T (1965) Glassy polymer diffusion is often tractable. Chem Eng News 43:64–65. https://doi.org/10.1021/cen-v043n041.p064

Ansari M, Mustafa S, Husain T, Ali R (2019) Water filtration using plant xylem in Northern India. IOP Conf Ser Mater Sci Eng 691:012037. https://doi.org/10.1088/1757-899X/691/1/012037

Austin J, Minelli C, Hamilton D, Wywijas M, Jones HJ (2020) Nanoparticle number concentration measurements by Multi-Angle dynamic light scattering. J Nanopart Res 22:108. https://doi.org/10.1007/s11051-020-04840-8

Aziz S, Mazhar AR, Ubaid A, Shah SMH, Riaz Y, Talha T, Jung DW (2024) A comprehensive review of membrane–based water filtration techniques. Appl Water Sci 14:169. https://doi.org/10.1007/s13201-024-02226-y

Berglund LA, Burgert I (2018) Bioinspired wood nanotechnology for functional materials. Adv Mater 30:1704285. https://doi.org/10.1002/adma.201704285

Berne BJ, Pecora R (2000) Dynamic light scattering. Courier Dover

Boutilier MSH, Lee J, Chambers V, Venkatesh V, Karnik R (2014) Water filtration using plant xylem. PLoS ONE 9:e89934. https://doi.org/10.1371/journal.pone.0089934

Cescon A, Jiang JQ (2020) Filtration process and alternative filter media material in water treatment. Water 12:3377. https://doi.org/10.3390/w12123377

Chen C, Kuang Y, Zhu S, Burgert I, Keplinger T, Gong A, Li T, Berglund L, Eichhorn SJ, Hu L (2020) Structure-Property-Function relationships of natural and engineered wood. Nat Rev Mater 5:642–666. https://doi.org/10.1038/s41578-020-0195-z

Chitaman K, Collado A, Decker M (2019) Xylem filter backpack. MANE J Student Res Innov Des 4:9–12

Choat B, Cobb AR, Jansen S (2008) Structure and function of bordered pits: new discoveries and impacts on Whole-Plant hydraulic function. New Phytol 177:608–626. https://doi.org/10.1111/j.1469-8137.2007.02317.x

Clayton GE, Thorn RMS, Reynolds DM (2021) The efficacy of chlorine-based disinfectants against planktonic and biofilm bacteria for decentralised point-of-use drinking water. Npj Clean Water 4:48. https://doi.org/10.1038/s41545-021-00139-w

Correa E, Sens ML (2002) Filtração de Água Em membranas de madeira - TCC [Water Filtration in Wood Membranes]. UFSC, Florianópolis, SC, pp 23–30

Fackler K, Thygesen LG (2013) Microspectroscopy as applied to the study of wood molecular structure. Wood Sci Technol 47:203–222. https://doi.org/10.1007/s00226-012-0516-5

Gwenaelle MPO, Jung J, Choi Y, Lee S (2017) Effect of microbubbles on microfiltration pretreatment for seawater reverse osmosis membrane. Desalination 403:153–160. https://doi.org/10.1016/j.desal.2016.06.012

Gwenzi W, Chaukura N, Noubactep C, Mukome FND (2017) Biochar-based water treatment systems as a potential low-cost and sustainable technology for clean water provision. J Environ Manag 197:732749. https://doi.org/10.1016/j.jenvman.2017.03.087

Hanief M, Zaman K, Ul Bashir S, Showkat J, Zubair M (2021) Investigation on Cypress wood membrane for water filtration. Bulg Chem Commun 53:25–31. https://doi.org/10.34049/bcc.53.D.10

Hashim A, Hashim NA, Junaidi MUM, Kamarudin D, Hussain MA (2022) Exploration of cassava plant xylem for water treatment: preparation, characterization and filtration capability. Water Sci Technol 86:1055–1065. https://doi.org/10.2166/WST.2022.253

Ibrahim N, Edri L, Bellizzi A, Kozlovsky C, Wiley M, Jacobitz FG, Fuller MG, Macdonald K, Bolender JP, Ruzaaza Ndaruhutse G, Lester Y (2022) Plant-based point-of-use water filtration: A simple solution for potable water in developing countries. Groundw Sustainable Dev 18:100802. https://doi.org/10.1016/j.gsd.2022.100802

Iwuozor KO (2019) Prospects and challenges of using Coagulation-Flocculation method in the treatment of effluents. Adv J Chem A 2:105–127. https://doi.org/10.29088/SAMI/AJCA.2019.2.105127

Jansen S, Choat B, Pletsers A (2009) Morphological variation of intervessel pit membranes and implications to xylem function in angiosperms. Am J Bot 96:409–419. https://doi.org/10.3732/AJB.0800248

Kabir AHME, Chakraborty TK, Ghosh GC (2016) Bio-Sand filter (BSF): A simple water treatment device for safe drinking water supply and to promote health in hazard prone Hard-to-Reach coastal areas of Bangladesh. Am J Environ Prot 5:107–112. https://doi.org/10.11648/j.ajep.20160505.11

Karim ME, Karim R, Islam MT, Muhammad-Sukki F, Bani NA, Muhtazaruddin MN (2019) Renewable energy for sustainable growth and development: an evaluation of law and policy of Bangladesh. Sustainability 11:5774. https://doi.org/10.3390/SU11205774

Khan MU, Khan MR (1984) Alum potash in water to prevent cholera. Lancet 3:1032. https://doi.org/10.1016/S0140-6736(84)91122-X

Lantagne DS, Quick R, Mintz ED (2006) Household water treatment and safe storage options in developing countries: a review of current implementation practices. In: Parker M, Williams A, Youngblood C (eds.) Water stories: expanding opportunities in small-scale water and sanitation projects (17-38). Woodrow Wilson International Center for Scholars: Environmental Change and Security Program. Retrieved February 10, 2008. https://www.wilsoncenter.org/publication/household-water-treatment-and-safe-storage-options-developing-countries-review-current

Londoño OM, Tancredi P, Rivas P, Muraca D, Socolovsky LM, Knobel M (2018) Small-Angle X-Ray scattering to analyze the morphological properties of nanoparticulated systems. In: Sharma S (ed) Handbook of materials characterization. Springer, Cham. https://doi.org/10.1007/978-3-319-92955-2_2

Mailer AG, Clegg PS, Pusey PN (2015) Particle sizing by dynamic light scattering: Non-Linear cumulant analysis. J Phys Condens Matter 27:145102. https://doi.org/10.1088/0953-8984/27/14/145102

McGuigan KG, Joyce TM, Conroy RM (1999) Solar disinfection: use of sunlight to decontaminate drinking water in developing countries. J Med Microbiol 48:785–787. https://doi.org/10.1099/00222615-48-9-785

Mdee OJ, Lwasa A, Sadiki N (2024) Overview of the Low-Cost technologies for household water treatment in developing countries. Water Pract Technol 19:3051. https://doi.org/10.2166/wpt.2024.177

Osseiran N, Lufadeju Y 18, WHO (2019) th, 1 in 3 People Globally Do Not Have Access to Safe Drinking Water– UNICEF,. https://www.who.int/news/item/18-06-2019-1-in-3-people-globally-do-not-have-access-to-safe-drinking-water-unicef-who

Pimentel CH, Freire MS, Gómez-Díaz D, González-Álvarez J (2023) Removal of wood dyes from aqueous solutions by sorption on untreated pine (Pinus Radiata) sawdust. Cellulose 30:4587–4608. https://doi.org/10.1007/s10570-023-05145-4

Plötze M, Niemz P (2011) Porosity and pore size distribution of different wood types as determined by mercury intrusion porosimetry. Eur J Wood Prod 69:649–657. https://doi.org/10.1007/s00107-010-0504-0

Pooi CK, Ng HY (2018) Review of Low-Cost Point-of-Use water treatment systems for developing communities. Npj Clean Water 1:11. https://doi.org/10.1038/s41545-018-0011-0

Potash BR (2014) Characterization and preservation techniques of plant xylem as low cost membrane filtration devices. MIT. https://dspace.mit.edu/handle/1721.1/92069

Ramchander K (2016) Development of Xylem-Based water filters. MIT. https://dspace.mit.edu/handle/1721.1/104270

Ramchander K (2021) Development of Fluidic Systems for Water Filtration and Bio-Separation. MIT. https://dspace.mit.edu/handle/1721.1/139001

Raval N, Maheshwari R, Kalyane D, Youngren-Ortiz SR, Chougule MB, Tekade RK (2019) Importance of physicochemical characterization of nanoparticles in pharmaceutical product development. Basic Fundamentals Drug Delivery 369–400. https://doi.org/10.1016/B978-0-12-817909-3.00010-8

Ruffinatto F, Negro F, Crivellaro A (2023) The macroscopic structure of wood. Forests 14:644. https://doi.org/10.3390/F14030644

Sánchez-Ferrer A, Merekalov A, Finkelmann H (2011) Opto-Mechanical effect in photoactive nematic Side-Chain Liquid-Crystalline elastomers. Macromol Rapid Commun 32:671–678. https://doi.org/10.1002/MARC.201100005

Sathish PS, Amuthan A (2012) Effect of soaking of Phyllanthus Emblica wood in Drinking-Water for purification. Int J Pharmacol Clin Sci 1:19–23. https://www.ijphs.org/article/2012/1/1-4

Selim Y, Mohamed A (2017) Role of dyestuff in improving Dye-Sensitized solar cell performance. RESD 3:79–82. https://doi.org/10.21622/RESD.2017.03.1.079

Sens ML, Emmendoerfer ML, Muller LC (2015) Water filtration through wood with helical Cross-Flow. Desalin Water Treat 53:15–26. https://doi.org/10.1080/19443994.2013.837010

Shanthamareen M, Wijeyaratne WMDN (2018) Efficacy of Phyllanthus Emblica Bark Powder in Reducing Total Hardness of Domestic Well Water in Jaffna Peninsula, Sri Lanka. *IRSPAS* p. 27. http://repository.kln.ac.lk/handle/123456789/19111

Sobsey MD, Stauber CE, Casanova LM, Brown JM, Elliott MA (2008) Point of use household drinking water filtration: a practical, effective solution for providing sustained access to safe drinking water in the developing world. Environ Sci Technol 42:4261–4267. https://doi.org/10.1021/es702746n

Sol D, Laca A, Laca A, Díaz M (2021) Microplastics in wastewater and drinking water treatment plants: occurrence and removal of microfibres. Appl Sci 11:10109. https://doi.org/10.3390/APP112110109

Soppe AIA, Heijman SGJ, Gensburger I, Shantz A, van Halem D, Kroesbergen J, Wubbels GH, Smeets PWMH (2015) Critical parameters in the production of ceramic pot filters for household water treatment in developing countries. J Water Health 13:587–599. https://doi.org/10.2166/wh.2014.090

Sperry JS (2003) Evolution of water transport and xylem structure. Int J Plant Sci 164:115–127. https://doi.org/10.1086/368398

Sperry JS, Hacke UG, Pittermann J (2006) Size and function in conifer tracheids and angiosperm vessels. Am J Bot 93:1490–1500. https://doi.org/10.3732/AJB.93.10.1490

Stjepanović M, Velić N, Galić A, Kosović I, Jakovljević T, Habuda-Stanić M (2021) From waste to biosorbent: removal of congo red from water by waste wood biomass. Water 13:279. https://doi.org/10.3390/w13030279

UN-Water (2021) Summary progress update 2021 – SDG 6 – Water and sanitation for all. Version: July 2021. Geneva, Switzerland

UNICEF (2020) Household water treatment filters - product guide: guidance on the selection and procurement of household filter for water treatment. https://www.unicef.org/supply/media/5221/file/%20household-water-treatment-filters-product-guide.pdf

Venkatesha R, Rao AB, Kedare SB (2020) Appropriate household point–of–use water purifier selection template considering a rural case study in Western India. Appl Water Sci 10:124. https://doi.org/10.1007/s13201-020-01207-1

Vitas S (2019) Chemical Modification of Wood Cross-Sections for Water Purification. ETH Zürich. In ETH Zurich Research Collection. https://doi.org/10.3929/ETHZ-B-000350865

Wiedenhoeft A, Eberhardt TL (2021) Structure and function of wood. Wood Handbook: wood as an engineering material: chapter 3. General Technical Report FPL-GTR-282. Madison, WI: U.S. Department of Agriculture, Forest Service, Forest Products Laboratory, p. 3.1-3.20. https://research.fs.usda.gov/treesearch/62242

World Health Organization (September (2023) 13th, Drinking-water. https://www.who.int/news-room/fact-sheets/detail/drinking-water